Soft Matter

Accepted Manuscript

ROYAL SOCIETY OF CHEMISTRY

www.rsc.org/softmatter

ARTICLE TYPE www. rsc.org/xxxxxx | XXXXXXXX

Coarse-grained treatment of the self-assembly of colloids suspended in a nematic host phase

Sergej Püschel-Schlotthauer,[a] Tillmann Stieger,[a] Michael Melle,[a] Marco G. Mazza,[b] and Martin Schoen[ac]

Received Xth XXXXXXXXXX 20XX, Accepted Xth XXXXXXXXX 20XX
First published on the web Xth XXXXXXXXXX 200X
DOI: 10.1039/b000000x

The complex interplay of molecular scale effects, nonlinearitites in the orientational field and long-range elastic forces makes the liquid-crystal physics very challenging. A consistent way to extract information from the microscopic, molecular scale up to the meso- and macroscopic scale is still missing. Here, we develop a hybrid procedure that bridges this gap by combining extensive Monte Carlo simulations, a local Landau-de Gennes theory, classical density functional theory, and finite-size scaling theory. As a test case to demonstrate the power and validity of our novel approach we study the effective interaction among colloids with Boojum defect topology immersed in a nematic liquid crystal. In particular, at sufficiently small separations colloids attract each other if the angle between their center-of-mass distance vector and the far-field nematic director is about 30°. Using the effective potential in coarse-grained two-dimensional MC simulations we show that self-assembled structures formed by the colloids ar in excellent agreement with experimental data.

1 Introduction

Liquid crystals are fluids made of molecules that lack spherical symmetry. Instead, their molecules contain elongated, rigid cores that form nematic liquid crystals, or disk-like cores that produce discotic liquid crystals or even more complex shapes. This simple property of anisotropy produces a myriad consequences for the optical, mechanical and thermodynamic properties of liquid crystals. For example, as the temperature is decreased they undergo a series of phase transitions where the symmetry of their state is spontaneously broken. Starting from a high temperature isotropic fluid, where all orientations are equivalent, to a nematic state where orientational order is broken, to a smectic phase, where positional order is broken in one dimension.

The molecular anisotropy produces effects on a macroscopic scale. In the nematic state, all molecules tend to align in the same direction, called the fluid's director.[1] But any localized deviation of molecular orientations from the director will cause a restoring, elastic force. However, a single global orientation cannot be satisfied for all boundary conditions. A colloid immersed in the nematic fluid causes a specific preferential alignment of the liquid crystal molecules on its surface, which is termed anchoring. A spherical colloid has a symmetry incompatible with a global nematic director. Thus, defects in the orientational field will arise. These topological defects are points or lines that minimize the free energy of the liquid crystal subject to complex boundary conditions. Depending on details of the fluid and the anchoring of its molecules at the colloid, the orientational field can be of such dazzling complexity that experts are just beginning to unravel its structural details.[2]

If multiple colloids are immersed in a nematic liquid crystal, the distortions of the local director field also give rise to effective interactions between the colloids mediated by the nemati host fluid.[3] These interactions may be used to self-assemble the colloids into supramolecular entities in a controlled (i.e., directed) manner. In this way ordered assemblies of colloids of an enormously rich structure with a great variety of symmetries may be built that would not otherwise exist without the ordered nature of the host phase.[4,5] These self-assembled coi loidal structures are also of practical importance, as they ca be used to produce photonic crystals.[6,7]

The forces guiding colloidal self-assembly result from a complex interplay of molecular scale ordering, mesoscopi elastic interactions, and large scale topological arguments While the framework of the Landau–de Gennes theory is appropriate for mesoscale effects, the elastic Frank–Oseen free energy is appropriate for long-range interactions.[8] However, there is a gap between the microscopic, molecular informa tion and the coarse-grained approaches used at the meso and

[a] *Stranski-Laboratorium für Physikalische und Theoretische Chemie, Fakultät für Mathematik und Naturwissenschaften, Technische Universität Berlin, Straße des 17. Juni 135, 10623 Berlin, Germany*
[b] *Max Planck Institut für Dynamik und Selbstorganisation, Am Faßberg 17, 37077 Göttingen, Germany*
[c] *Department of Chemical and Biomolecular Engineering, Engineering Building I, Box 7905, North Carolina State University, 911 Partners Way, Raleigh, NC 27695, U.S.A.*

macroscopic scale. No consistent method exists to transfer physical information from the molecular scale up to the scale where elastic forces and nonlinearities in the nematic interactions occur. Here, we pursue the goal of bridging this gap. The task is not idle, as there are physical situations that have so far eluded a precise explanation at the molecular level. As a test case to demonstrate power and validity of a novel hybrid approach developed in this work we take on the problem of colloidal self-assembly. Poulin and Weitz[9] found experimentally that in a nematic phase the colloidal center-to-center distance vector $\boldsymbol{r}_{12}$ forms a "magic" angle of $\theta \approx 30^\circ$ with the global director $\widehat{\boldsymbol{n}}_0$ if the liquid crystal molecules (mesogens) favor a local planar anchoring at the colloid's surface.[10]

Near an isolated colloid with planar anchoring the mesogens will produce a Boojum defect. While for such a single topological defect long-range approximation analogous to electrostatics can be sufficient, the complex interaction of multiple Boojum defects requires a more careful analysis. In previous theoretical attempts a much larger angle of about 50° is usually found.[9,11] This number is based upon calculations where one employs the electrostatic analog of the Boojum defect topology.[9] In fact, as stated explicitly by Poulin and Weitz "*This theoretical value is different from the experimentally observed value for θ ... since the theory is a long-range description that does not account for short-range effects*".[9]

Theoretical results similar to the experimental ones by Poulin and Weitz[9] were recently found by Tasinkevych *et al.* through a direct minimization of a Landau-de Gennes free-energy functional.[8] These authors demonstrate that the radial component of the elastic force has an attractive minimum around $\theta \approx 30^\circ$ for certain $r_{12} = |\boldsymbol{r}_{12}|$; this minimum shifts to larger θ as r_{12} increases. However, to date and to the best of our knowledge no molecular-scale work exists supporting the result of Tasinkevych *et al.*[8] or the experimental findings by Poulin and Weitz[9].

Another motivation for our work is the more recent experimental observation that between a pair of colloids in a nematic host repulsive and attractive forces act depending on θ.[11] For example, at $\theta \approx 30^\circ$ the colloids attract each other whereas at $\theta = 0^\circ$ and 90° repulsion between the colloids is observed.

To study these effects starting from a molecular-level based description we employ a combination of Monte Carlo (MC) simulations in the isothermal-isobaric and canonical ensembles, two-dimensional (2D), coarse-grained MC simulations in the canonical ensemble, classical density functional theory (DFT), concepts of finite-size scaling (FSS), and Landau-de Gennes (LdG) theory to investigate the effective interaction between a pair of spherical, chemically homogeneous colloids mediated by a nematic host phase.

The remainder of this manuscript is organized as follows. We begin in Section 2 with an introduction of our model system and its various constituents. Relevant theoretical concepts are introduced in Section 3. In Section 4 we present results of this study which we summarize and discuss in the closing Section 5 of this manuscript.

2 Model

In this work we consider the self-assembly of colloidal particles in two and three dimensions. The colloids are immersed in a nematic liquid-crystalline host fluid where an external field is invoked to control the global director $\widehat{\boldsymbol{n}}_0$. The following three sections are devoted to introducing the various constituents of our model and to specifying their interactions with one another.

2.1 Host phase

The liquid crystal host phase is composed of N mesogens interacting with each other in a pairwise additive fashion. The interaction potential can be cast as

$$\varphi_{\rm mm}\left(\boldsymbol{r}_{ij},\omega_i,\omega_j\right) = \varphi_{\rm iso}\left(r_{ij}\right) + \varphi_{\rm anis}\left(\boldsymbol{r}_{ij},\omega_i,\omega_j\right) \qquad (1)$$

where $\boldsymbol{r}_{ij} = \boldsymbol{r}_i - \boldsymbol{r}_j$ is the distance vector conncecting the centers of mass of a mesogenic pair located at points $\boldsymbol{r}_i$ and $\boldsymbol{r}_j$, respectively, and $r_{ij} = \left|\boldsymbol{r}_{ij}\right|$. According to eqn. (1) the full interaction potential is split into an isotropic ($\varphi_{\rm iso}$) and an anisotropic part ($\varphi_{\rm anis}$) where the latter depends on the orientations ω_i and ω_j of the mesogenic pair. In fact, $\omega_{i,j} = (\theta_{i,j},\phi_{i,j})$ where $\theta_{i,j}$ and $\phi_{i,j}$ are Euler angles implying that the mesogens have uniaxial symmetry.

For the isotropic contribution we adopt the well-known Lennard-Jones potential

$$\varphi_{\rm iso}\left(r_{ij}\right) = 4\varepsilon_{\rm mm}\left[\left(\frac{\sigma}{r_{ij}}\right)^{12} - \left(\frac{\sigma}{r_{ij}}\right)^{6}\right] = \varphi_{\rm rep}\left(r_{ij}\right) + \varphi_{\rm att}\left(r_{ij}\right) \qquad (2)$$

where $\varepsilon_{\rm mm}$ is the depth of the attractive well, σ is the van der Waals diameter of the isotropic core, and $\varphi_{\rm rep}$ and $\varphi_{\rm att}$ represent repulsive and attractive contributions to $\varphi_{\rm iso}$, respectively.

To derive an expression for the anisotropic contribution in eqn. (1) we follow Giura and Schoen.[12] From a lengthy but relatively straightforward derivation these authors show that

$$\varphi_{\rm anis}\left(\boldsymbol{r}_{ij},\omega_i,\omega_j\right) = \varphi_{\rm att}\left(r_{ij}\right)\Psi\left(\widehat{\boldsymbol{r}}_{ij},\omega_i,\omega_j\right) \qquad (3)$$

In eqn. (3) the anisotropy function is given by

$$\begin{aligned}\Psi\left(\widehat{\boldsymbol{r}}_{ij},\omega_i,\omega_j\right) &= 5\varepsilon_1 P_2\left[\widehat{\boldsymbol{u}}\left(\omega_i\right)\cdot\widehat{\boldsymbol{u}}\left(\omega_j\right)\right] \\ &\quad +5\varepsilon_2\left\{P_2\left[\widehat{\boldsymbol{u}}\left(\omega_i\right)\cdot\widehat{\boldsymbol{r}}_{ij}\right] + P_2\left[\widehat{\boldsymbol{u}}\left(\omega_j\right)\cdot\widehat{\boldsymbol{r}}_{ij}\right]\right\}\end{aligned} \qquad (4)$$

where $\widehat{\boldsymbol{u}}\left(\omega_{i,j}\right)$ and $\widehat{\boldsymbol{r}}_{ij} = \boldsymbol{r}_{ij}/r_{ij}$ are unit vectors specifying the orientation of mesogens i and j and the orientation of the

center-of-mass distance vector, respectively, both in a space-fixed frame of reference. In addition, $P_2(x) = \frac{1}{2}\left(3x^2-1\right)$ is the second Legendre polynomial and the (dimensionless) anisotropy parameters $2\varepsilon_1 = -\varepsilon_2 = -0.08$ are fixed throughout this work. Notice also that the first term on the right-hand side of eqn. (4) matches the orientation dependence of interactions in the Maier-Saupe model[13,14] whereas the next two terms account for the anisotropy of mesogen-mesogen attractions with enhanced sophistication.

2.2 External field

For a suitable choice of thermodynamic state parameters the host phase introduced in Section 2.1 exhibits isotropic liquid and nematic phases.[12] Unfortunately, when a nematic phase is forming in the bulk it is impossible to determine beforehand the direction of $\widehat{\boldsymbol{n}}_0$. In fact, there is an infinite number of easy axes[15] with which $\widehat{\boldsymbol{n}}_0$ may align in the bulk nematic phase.

To predict and control $\widehat{\boldsymbol{n}}_0$ it has therefore become customary to place the liquid crystal between solid substrates with specially prepared surfaces that tend to align mesogens in their vicinity in a desired way.[16] Because orientational order in a nematic liquid crystal is a long-range phenomenon, substrate-induced alignment of mesogens allows one to control $\widehat{\boldsymbol{n}}_0$ on a length scale exceeding by far a molecular one. A host of different techniques to achieve a particular substrate anchoring of mesogens experimentally has been known for quite some time.[17]

In this work we take the substrates to be planar and structureless such that their surfaces are separated by a distance s_z along the z-axis. Thus, the interaction between a mesogen and the substrates can be cast as

$$\varphi_{\rm ms}(z_i,\omega_i) = \varepsilon_{\rm ms}\left[\frac{2}{5}\left(\frac{\sigma}{\Delta z_i}\right)^{10} - \left(\frac{\sigma}{\Delta z_i}\right)^{4} g(\omega_i)\right] \qquad (5)$$

where $\Delta z_i = z_i \pm s_z/2$ is the distance of mesogen i from the lower $(+)$ and upper $(-)$ substrate plane, respectively. Hence, $\varphi_{\rm ms}$ may be viewed as a local, orientation dependent external field, the strength of which is controlled by $\varepsilon_{\rm ms}$. Throughout this work we take $\varepsilon_{\rm ms}/\varepsilon_{\rm mm} = 5.00$.

The value of $\varepsilon_{\rm ms}$ is chosen for two reasons. First, it guarantees a sufficiently strong alignment of mesogens with the surface so that fluctuation of $\widehat{\boldsymbol{n}}_0$ over the course of the simulations are negligible. Second, $\varepsilon_{\rm ms}$ is still small enough to prevent from freezing those portions of the host phase that are located in the vicinity of the substrates.

The orientation dependence of the external field in our model enters through the anchoring function

$$g(\omega_i) = [\widehat{\boldsymbol{u}}(\omega_i)\cdot\widehat{\boldsymbol{e}}_{\rm x}]^2 \qquad (6)$$

where $\widehat{\boldsymbol{e}}_{\rm x}$ is a unit vector parallel to the x-axis. Hence, the anchoring function discriminates energetically between a desired orientation of mesogens parallel with this axis and less desired ones for which $|\widehat{\boldsymbol{u}}(\omega_i)\cdot\widehat{\boldsymbol{e}}_{\rm x}| < 1$. In other words, $g(\omega_i)$ may be viewed as a mathematical "device" mimicking aligning substrates in experimental setups. On account of its definition in eqn. (6), $g(\omega_i)$ allows one to more or less pin $\widehat{\boldsymbol{n}}_0$ to the x-axis *on average* where $|\widehat{\boldsymbol{n}}_0\cdot\widehat{\boldsymbol{e}}_{\rm x}| \simeq 1$ due to thermal fluctuations.

2.3 Colloidal particles

In addition, colloidal particles are immersed into the nematic liquid crystal. These colloids are spherical in shape, where $r_0 = 3.00\sigma$ is their hard-core radius, and have a chemically homogeneous surface. Similar to the planar substrates we envision the surfaces of the colloids to have been treated such that mesogens have a specific orientation with respect to the local surface normal of a colloid. Following earlier work by some of us[18] we take the mesogen-colloid interaction potential to be given by

$$\varphi_{\rm mc}(\boldsymbol{r}_i,\omega_i) = \varepsilon_{\rm mc}\left[a_1\left(\frac{\sigma}{r_{ij}^{\rm c}-r_0}\right)^{10} - a_2\frac{\exp\left[-\eta\left(r_{ij}^{\rm c}-r_0\right)\right]}{r_{ij}^{\rm c}-r_0} g_{\rm c}\left(\widehat{\boldsymbol{r}}_{ij}^{\rm c},\omega_i\right)\right] \qquad (7)$$

where $r_{ij}^{\rm c} = \left|\boldsymbol{r}_i - \boldsymbol{r}_j^{\rm c}\right|$ is the distance between the center of mass of mesogen i at $\boldsymbol{r}_i$ and that of colloid j at $\boldsymbol{r}_j^{\rm c}$. Hence, $r_{ij}^{\rm c} - r_0$ is the distance of the center of mass of mesogen i from the surface of colloid j. The strength of the mesogen-colloid interaction is controlled by $\varepsilon_{\rm mc}$ which we maintain constant so that $\varepsilon_{\rm mc}/\varepsilon_{\rm mm} = 3.50$. Again, this value has been selected on the basis of the same rationale given in Section 2.2.

In eqn. (7), η is the inverse Debye screening length and parameters a_1 and a_2 have been introduced to guarantee that the minimum of $\varphi_{\rm mc}$ remains at a distance $r_0+\sigma$ from the colloid's center of mass and to maintain the depth of the attractiv well at $\varepsilon_{\rm mc}$ irrespective of η.[18] Throughout this work we fix $\eta\sigma = 0.50$.

Last but not least, we introduce another anchoring function in eqn. (7) which we take to be given by

$$g_{\rm c}\left(\widehat{\boldsymbol{r}}_{ij}^{\rm c},\omega_i\right) = \left[1 - \left|\widehat{\boldsymbol{r}}_{ij}^{\rm c}\cdot\widehat{\boldsymbol{u}}(\omega_i)\right|\right]^2 \qquad (8)$$

where $\widehat{\boldsymbol{r}}_{ij}^{\rm c} = \boldsymbol{r}_{ij}^{\rm c}/r_{ij}^{\rm c}$ is the local surface normal of the colloid. Hence, the anchoring function introduced in eqn. (8) serves to align mesogens in a degenerate[15], locally planar fashion wit respect to the colloid's surface.

3 Theory

To eventually simulate the self-assembly of several colloidal particles in a coarse-grained fashion we seek to represent the

nematic host phase through an effective interaction potential. Key to this approach (as in all coarse-grained treatments) is a sensible protocol to integrate out irrelevant degrees of freedom while preserving the correct physics. Here, we seek to link a molecular-level description of the nematic host to a continuum treatment.

3.1 Continuum approach

As already pointed out in Section 1, the presence of a colloid in a nematic liquid crystal causes $\widehat{\boldsymbol{n}}(\boldsymbol{r})$ to deviate from $\widehat{\boldsymbol{n}}_0$ in certain regions near the colloid's surface. Associated with this distortion of $\widehat{\boldsymbol{n}}(\boldsymbol{r})$ is a local deviation between the nematic order parameter and its bulk value in the absence of any colloid. Both, the distortion of $\widehat{\boldsymbol{n}}(\boldsymbol{r})$ and the associated decline of $S(\boldsymbol{r})$ cause changes in the free energy of the composite system (i.e., colloid plus nematic host). Adopting a continuum perspective a key quantity is the local alignment tensor $\mathbf{Q}(\boldsymbol{r})$ whose components can be cast as

$$Q_{\alpha\beta}(\boldsymbol{r}) = \frac{S(\boldsymbol{r})}{2}\left[3n_\alpha(\boldsymbol{r})n_\beta(\boldsymbol{r}) - \delta_{\alpha\beta}\right] \tag{9}$$

where $S(\boldsymbol{r})$ is the nematic order parameter, $n_\alpha(\boldsymbol{r})$ is the α-component of $\widehat{\boldsymbol{n}}(\boldsymbol{r})$, and $\delta_{\alpha\beta}$ is the Kronecker symbol. The assumption underlying eqn. (9) is that a spatial variation of the degree of nematic order of uniaxial symmetry and a deformation of the nematic director field are coupled (see also Section 4.4) .

Therefore, the total change in free-energy density may readily be expressed as

$$\Delta f(\boldsymbol{r}) = \Delta f_{\mathrm{LdG}}(\boldsymbol{r}) + f_{\mathrm{el}}(\boldsymbol{r}) + f_{\mathrm{core}} \tag{10}$$

where the Landau-de Gennes contribution is given by

$$\begin{aligned}\Delta f_{\mathrm{LdG}}(\boldsymbol{r}) &= \frac{A}{2}Q_{\alpha\beta}Q_{\beta\alpha} + \frac{B}{3}Q_{\alpha\beta}Q_{\beta\gamma}Q_{\gamma\alpha} + \frac{C}{4}\left(Q_{\alpha\beta}Q_{\beta\alpha}\right)^2 \\ &\quad -\Delta f_0\end{aligned} \tag{11}$$

using Einstein's summation convention. Equation (11) is essentially a Taylor expansion of the free-energy density in terms of the order parameter tensor at the isotropic-nematic (IN) phase transition. In eqn. (11), A, B, and C are unknown expansion coefficients depending only on density ρ and temperature T. Assuming uniaxiality, we employ the identities $Q_{\alpha\beta}Q_{\beta\alpha} = \frac{3}{2}S$ and $Q_{\alpha\beta}Q_{\beta\gamma}Q_{\gamma\alpha} = \frac{3}{4}S^3$ This allows us to rewrite eqn. (11) as

$$\Delta f_{\mathrm{LdG}}(\boldsymbol{r}) = \frac{3}{4}AS^2(\boldsymbol{r}) + \frac{1}{4}BS^3(\boldsymbol{r}) + \frac{9}{16}CS^4(\boldsymbol{r}) - \Delta f_0 \tag{12}$$

To simplify the notation we also temporarily dropped the argument $\boldsymbol{r}$ of the components of $\mathbf{Q}(\boldsymbol{r})$ on the righthand side of eqn. (11).

In eqn. (11) as well as in eqn. (12)

$$\Delta f_0 = AS_{\mathrm{b}}^2 + BS_{\mathrm{b}}^3 + CS_{\mathrm{b}}^4 \tag{13}$$

is a similar LdG free-energy density of the nematic host phase obtained for the same T and ρ but in the absence of colloids and relative to the free-energy density of a corresponding isotropic fluid. In eqn. (13), S_{b} is the (global) bulk nematic order parameter. To arrive at the expression in eqn. (13) the same identities linking products of the alignment tensor to the nematic order parameter have been used as before.

Next, the elastic contribution to Δf in the one-constant approximation (see below) may be cast as

$$\begin{aligned}f_{\mathrm{el}}(\boldsymbol{r}) &= \frac{L}{2}\left(\partial_\gamma Q_{\alpha\beta}\right)\left(\partial_\gamma Q_{\beta\alpha}\right) \\ &= \frac{3}{4}L\left[\nabla S(\boldsymbol{r})\right]^2 + \frac{K}{2}\left\{\left[\nabla\cdot\widehat{\boldsymbol{n}}(\boldsymbol{r})\right]^2 + \left[\nabla\times\widehat{\boldsymbol{n}}(\boldsymbol{r})\right]^2\right\} \\ &= \frac{3}{4}L\left[\nabla S(\boldsymbol{r})\right]^2 + f_{\mathrm{FO}}(\boldsymbol{r})\end{aligned} \tag{14}$$

where $f_{\mathrm{FO}}(\boldsymbol{r})$ is the (local) Frank-Oseen free-energy density and eqn. (9) has also been used. In eqn. (14), L is an elastic and K is the Frank constant. The two are related via

$$K = \frac{9}{2}LS^2(\boldsymbol{r}) \tag{15}$$

To apply eqn. (14) some caution is advisable. This is because the expression for $f_{\mathrm{FO}}(\boldsymbol{r})$ in eqn. (14) is derived under the assumption that spatial variations of $\widehat{\boldsymbol{n}}(\boldsymbol{r})$ occur on a length scale that is large compared to a molecular one. As we shall demonstrate below this is true in our system almost everywhere except inside the core of defects. To avoid an improper calculation of $f_{\mathrm{FO}}(\boldsymbol{r})$ we restrict the evaluation of eqn. (14) to regions *outside* the defect core.[19–21] The latter is defined through the inequality $S(\boldsymbol{r}) \leq S_{\mathrm{IN}}$ where S_{IN} is the nematic order parameter at the IN phase transition in the host phase (and in the absence of any colloidal particle; see below).

Because we are restricting the use of eqn. (14) by "cutting out" the defect core some correction to Δf due to the core region is required. As pointed out by de las Heras *et al.* it is necessary to include such a correction to the change in free-energy density because of the nanoscopic size of our colloidal particle.[22] This correction, represented by f_{core} in eqn. (10), will be discussed in some in Section 4.3.

Last but not least, we emphasize that within the framework of the present continuum theory the standard approach is to minimize the functional[23]

$$\Delta\mathscr{F}\left[S(\boldsymbol{r}),\widehat{\boldsymbol{n}}(\boldsymbol{r})\right] = \int \mathrm{d}\boldsymbol{r}\,\Delta f\left[S(\boldsymbol{r}),\widehat{\boldsymbol{n}}(\boldsymbol{r})\right] \tag{16}$$

However, this procedure has a twofold drawback. First, the minimization bears the danger that its solutions $S(\boldsymbol{r})$ and $\widehat{\boldsymbol{n}}(\boldsymbol{r})$

do not necessarily correspond to the global minimum of $\Delta\mathscr{F}$. This is in particular so if the structure of $S(\boldsymbol{r})$ and $\widehat{\boldsymbol{n}}(\boldsymbol{r})$ in thermodynamic equilibrium is rather complex.[24] Second, there is no way within the framework of the continuum approach to determine the material constants A, B, C, and K (or L). Here one usually resorts to experimental information which is available for a few liquid crystals.[25]

In closing, we emphasize that the expressions given in eqn. (12) and eqn. (14) correspond to the same ground state. For example, in the absence of any perturbation, that is if $S(\boldsymbol{r}) = S_\mathrm{b}$ and $\widehat{\boldsymbol{n}}(\boldsymbol{r}) = \widehat{\boldsymbol{n}}_0$, $\Delta f_\mathrm{LdG} = f_\mathrm{el} = 0$.

3.2 Molecular approach

3.2.1 Basic properties. Here we pursue an alternative approach based upon a molecular picture of the host phase and suitable for implementation in MC simulations. If carried out according to the acknowledged rules of the art, MC gives us immediate access to $S(\boldsymbol{r})$ and $\widehat{\boldsymbol{n}}(\boldsymbol{r})$ for a thermodynamic equilibrium situation via suitably defined ensemble averages. One may then feed $S(\boldsymbol{r})$ and $\widehat{\boldsymbol{n}}(\boldsymbol{r})$ into expressions such as eqn. (12) and eqn. (14) to eventually obtain the absolute minimum of $\Delta\mathscr{F}$ [after an integration of $\Delta f(\boldsymbol{r})$ over volume, see also Section 4.3].

Thus, to eventually compute $\Delta\mathscr{F}$ we begin by introducing the local alignment tensor

$$\mathbf{Q}(\boldsymbol{r}) = \frac{1}{2\rho(\boldsymbol{r})}\left\langle \sum_{i=1}^{N} \left[3\widehat{\boldsymbol{u}}(\omega_i)\widehat{\boldsymbol{u}}(\omega_i) - \mathbf{1}\right]\delta(\boldsymbol{r}_i - \boldsymbol{r})\right\rangle \qquad (17)$$

at the molecular level where $\mathbf{1}$ is the unit tensor and $\langle\ldots\rangle$ denotes an ensemble average.[18,26] In eqn. (17), $\rho(\boldsymbol{r})$ is the local number density. Because $\mathbf{Q}(\boldsymbol{r})$ can be represented by a 3×3 matrix it has three eigenvalues which we obtain numerically using Jacobi's method.[27] We take the largest eigenvalue of $\mathbf{Q}(\boldsymbol{r})$ as the local nematic order parameter $S(\boldsymbol{r})$ and the associated eigenvector as the nematic director field $\widehat{\boldsymbol{n}}(\boldsymbol{r})$.

However, to compute $\Delta f_\mathrm{LdG}(\boldsymbol{r})$ and $f_\mathrm{el}(\boldsymbol{r})$ the material constants A, B, C, and K are required. Whereas this is relatively straightforward within the framework of MC simulations as far as K is concerned, one encounters serious difficulties to compute A, B, and C reliably. We address these difficulties below.

For the calculation of K we employ a method suggested by Allen and Frenkel.[28,29] In their approach one considers fluctuations of Fourier components $\widetilde{\mathbf{Q}}(\boldsymbol{k})$ of $\mathbf{Q}(\boldsymbol{r})$. In the limit of $|\boldsymbol{k}| \to 0$ simple linear relationships exist from which the Frank constants K_1, K_2, and K_3 associated with bend, twist, and splay deformations of $\widehat{\boldsymbol{n}}(\boldsymbol{r})$ can be estimated reliably. Stieger *et al.*[30] have recently applied the method of Allen and Frenkel[28,29] to show that for the present model of the host phase $K_1 \simeq K_2 \simeq K_3 = K$ so that the one-constant form[1] of f_el in eqn. (14) is an excellent approximation. Under the thermodynamic conditions used here (see Section 4.1), $K \simeq 1.66\varepsilon_\mathrm{mm}\sigma^{-1}$ is obtained.

3.2.2 Classical density functional theory. To compute A, B, and C the situation is more difficult. In principle, one could obtain these constants from the order-parameter distribution $P(S_\mathrm{b})$ obtained for a bulk nematic phase without colloidal particles. However, as discussed in detail by Eppenga and Frenkel[26] and later by Greschek and Schoen[31] it is next to impossible to determine B and C with sufficient statistical accuracy from $P(S_\mathrm{b})$.

We therefore resort to a different approach based upon classical mean-field DFT. As demonstrated elsewhere[32] the change in free energy-density of the bulk nematic relative to the isotropic phase can be cast as

$$\beta\Delta f_\mathrm{n} = \rho\int_{-1}^{1}\mathrm{d}x\,\overline{\alpha}(x)\ln\left[2\overline{\alpha}(x)\right] + \rho^2\sum_{\substack{l=2\\ l\ \mathrm{even}}} S_l^2 u_l \qquad (18)$$

where $\beta = 1/k_\mathrm{B}T$ (k_B is Boltzmann's constant), $x = \cos\theta$, and θ is the azimuthal angle if we take the z-axis of our coordinate system to coincide with $\widehat{\boldsymbol{n}}_0$. Members of the set $\{S_l\}$ defined on the interval $[0,1]$ are order parameters and $\{u_l\}$ are parameters that account for the contribution of anisotropic mesogen-mesogen interactions to the free energy, respectively.[32]

The integrand on the right-hand side of eqn. (18) contains the orientation distribution function $\overline{\alpha}(x)$. It depends only on θ due to the uniaxial symmetry of the nematic phase and is normalized according to

$$\int_{-1}^{1}\mathrm{d}x\,\overline{\alpha}(x) = 1 \qquad (19)$$

which implies that in the isotropic phase $\overline{\alpha}(x) = \frac{1}{2}$. Again, because of the uniaxiality of the nematic phase we expand $\overline{\alpha}(x)$ in terms of Legendre polynomials $\{P_l\}$ via

$$\overline{\alpha}(x) = \frac{1}{2} + \sum_{\substack{l=2\\ l\ \mathrm{even}}}\frac{2l+1}{l}S_l P_l(x) = \frac{1}{2} + \xi(x) \qquad (20)$$

Inserting this expression into eqn. (18), expanding the integrand in a Taylor series around $\xi = 0$ (i.e., at the IN phase transition), and retaining in this expansion terms up to $\mathscr{O}(\xi^4)$ allows us to recast eqn. (18) as

$$\Delta f_\mathrm{n} = \underbrace{a(\rho)(T - T^*)}_{A}S_\mathrm{b}^2 - \frac{32\rho k_\mathrm{B}T}{105}S_\mathrm{b}^3 + \frac{64\rho k_\mathrm{B}T}{315}S_\mathrm{b}^4 \qquad (21)$$

if we limit ourselves to the leading term $l = 2$ in the expression for ξ and use $S_2 = S_\mathrm{b}$. In eqn. (21), $a = 2\rho k_\mathrm{B}/5$ and

$T^* = -5\rho u_2/2k_B$ where the latter is the temperature at which the isotropic phase becomes thermodynamically unstable. Assuming $\Delta f_n = \Delta f_0$ one easily obtains

$$B = -\frac{8\rho k_B T}{105} \quad (22a)$$

$$C = \frac{4\rho k_B T}{35} \quad (22b)$$

by comparing terms of equal power in S_b in eqn. (21) with corresponding ones in eqn. (13). Hence, $B < 0$, $C > 0$, and A changes sign at $T = T^*$ as it is to be expected at the IN phase transition.[1]

3.2.3 Elements of finite-size scaling theory. Unfortunately, the expression for T^* given in the preceding section depends on u_2 which in itself depends on the level of sophistication at which pair correlations are treated within mean-field DFT. For example, at simple mean-field (SMF) level, where one completely ignores pair correlations, $u_2 = -32\pi\varepsilon_1\varepsilon_{mm}/15$. A more elaborate, temperature dependent form for u_2 obtains at so-called modified mean-field (MMF) level [see eqn. (3.7) and eqn. (3.8) of Ref.[12]] where one takes into account pair correlations to some extent via an orientation-dependent Mayer f-function.

Unfortunately, at SMF level T^* turns out to be grossly underestimated whereas at MMF level its value is equally grossly overestimated as a previous FSS study of the IN phase transition suggests.[31] This failure can be linked to the complete neglect of pair correlations at SMF level and their overestimation in liquidlike phases at MMF level.[12]

To improve this situation we pursue a different approach invoking concepts of FSS theory. First, within LdG theory it is a relatively simple matter to show that[33]

$$T_{IN} = T^* + \frac{1}{27}\frac{B^2}{aC} \quad (23)$$

Second, with an improved estimate for T_{IN} and coefficients for a, B, and C from DFT one can hope to obtain an improved estimate for T^* from the above expression.

In FSS theory one makes explicit use of the fact that in any molecular simulation one is always confronted with systems of finite extent. Considering moments

$$\overline{S_b^n} = \int_0^1 \mathrm{d}S_b\, S_b^n P(S_b) \quad (24)$$

of the order-parameter distribution the key quantity in FSS are cumulants of its various moments. Here, the second-order cumulant

$$g_2 = \frac{\overline{S_b^2}}{\overline{S_b}^2} \quad (25)$$

is particularly useful.[31] If a phase transition is discontinuous *in principle* (as the IN phase transition) but rounded on accout of the finiteness of the system under study one anticipates pairs of cumulants for different system sizes to have a common intersection[31] which scales as $\mathscr{L}^{-d}$ where $\mathscr{L}$ is the linear extent of a system of dimension d.[34]

Moreover, it has been demonstrated by Vollmayer *et al.*[35] that the "distance" of a unique cumulant intersection from the point at which the phase transition would occur in the thermodynamic limit scales as $\mathscr{L}^{-2d}$. Thus, one can expect that for sufficiently large systems it may seem that even at a discontinuous phase transition all cumulants intersect in a unique point which then for all practical purposes may be taken as the state point at which the phase transition would occur in the thermodynamic limit.

4 Results

4.1 Numerical details

Our results are based upon MC simulations in a specialized isothermal-isobaric ensemble discussed in detail elsewhere.[18] In this ensemble a thermodynamic state is specified by N, T, the ratio of side lengths of the simulation cell in the x- and y-directions s_x/s_y, the distance s_z between the solid substrates, and the transverse component $P_\parallel = \frac{1}{2}\left(P_{xx} + P_{yy}\right)$ of the pressure tensor $\mathbf{P}$. The specialized isothermal-isobaric ensemble is employed to equilibrate the system. Production runs were carried out in the canonical ensemble using the average side lengths from the isothermal-isobaric equilibration run as fixed input values.[36]

We generate a Markov chain by a conventional Metropolis protocol where it is decided with equal probability whether to displace a mesogen's center of mass by a small amount or to rotate the mesogen around a randomly chosen axis. All mesogens are considered sequentially such that a MC cycle commences once each of the N mesogens has been subjected to either a displacement or rotation attempt.

Our results are typically based upon 1.5×10^5 MC cycles for equilibration followed by another 1.0×10^6 cycles during which relevant ensemble averages are taken. To save computer time we cut off mesogen-mesogen interactions beyond center-of-mass separations $r_c = 3.00\sigma$. In addition, we employ a combination of a Verlet and link-cell neighborlist. A mesogen is considered a neighbor of a reference mesogen if their centers of mass are separated by less than $r_N = 3.50\sigma$.

As we are not interested in simulating any particular material we express all quantities in dimensionless (i.e., "reduced") units. For example, energy is given in units of ε_{mm}, length in units of σ, and temperature in units of ε_{mm}/k_B. Other derived units are obtained as suitable combinations of these basic ones (see Appendix B.1 of the book by Allen and Tildesley[37]).

We consider a thermodynamic state characterized by $T = 0.95$ and $P_{\|} = 1.80$ corresponding to a mean number density $\rho \simeq 0.92$ for which the host phase is sufficiently deep in the nematic phase indicated by $S_b \simeq 0.70$. For all the simulations and regardless of the spatial arrangement of the colloidal pair we take $s_z = 24.0$ so that the immediate environment of the colloids is not affected directly by the presence of the solid substrates whose sole purpose is to fix $\widehat{\boldsymbol{n}}_0$.

4.2 Bulk phase

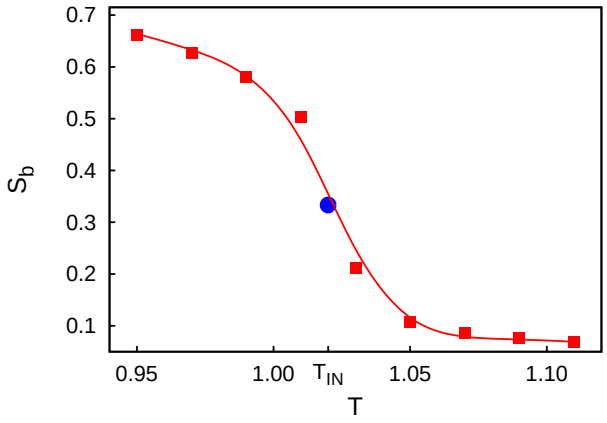

Fig. 1 Plot of the nematic order parameter S_b as a function of temperature T (■). Data are shown for $N = 1000$ mesogens. The IN phase transition occurs at T_{IN} and is obtained from an analysis of the second-order cumulant (see text). The full line represents a spline fitted to the discrete data points and intended to guide the eye. Also shown is $S_{IN} = \frac{1}{3}$ at T_{IN} predicted by LdG theory (●) (see text).

We begin our presentation of properties of the bulk phase in the absence of any colloidal particle. To illustrate that under the thermodynamic conditions chosen the host fluid is in the nematic phase we present in Figure 1 a plot of S_b across the IN phase transition. Because of the relatively small system size the IN phase transition appears to be rounded despite its *in principle* discontinuous character.

Another well-known finite-size effect is visible in the isotropic phase (i.e., for $T > T_{IN}$) where S_b approaches a small nonzero plateau value of about 0.069. This can be explained by assuming that the liquid crystal consists of molecular-size domains in which mesogens align their longer axes preferentially because of the form of φ_{mm}. In the isotropic phase these domains are uncorrelated. However, their number is finite so that by averaging S_b over the ordered domains a residual nonzero value is obtained.

At this stage it is noteworthy that finite system size affects the nematic order parameter only in the isotropic phase and near the IN phase transition [see, for example, Figure 6(b) of Ref.[12] or Figure 2(b) of Ref.[31]] whereas S_b is insensitive to system size sufficiently deep in the nematic phase. Hence, under the present thermodynamic conditions (see Section 4.1) a significant system-size effect is not anticipated for the pure host phase (i.e., in the absence of colloidal particles). The presence of the colloids will cause formation of nearly isotropic domains of a certain size determined by the surface curvature of the colloidal particle (i.e., by its size). In these domains, $S(\boldsymbol{r})$ is small but nonzero. However, size and shape of the domains and the actual value of $S(\boldsymbol{r})$ reflect the true physics of the system and should not be confused with finite-size effects in the bulk and in the absence of the colloids as discussed before.

Another feature illustrated by the plot in Figure 1 is that the value predicted by LdG theory

$$S_{IN} = -\frac{2}{9}\frac{B}{C} = \frac{1}{3} \tag{26}$$

agrees remarkably well with $S_{IN} \simeq 0.36$ obtained from MC using FSS (see below). Moreover, S_{IN} from LdG theory turns out to be universal in that it neither depends on ρ nor T. This is similar to Maier-Saupe theory where a similar universal value is found.[38] However, more recent MMF DFT calculations showed that instead S_{IN} exhibits a temperature dependence such that a limiting value of S_{IN} is approached from above if T_{IN} is sufficiently high.[12]

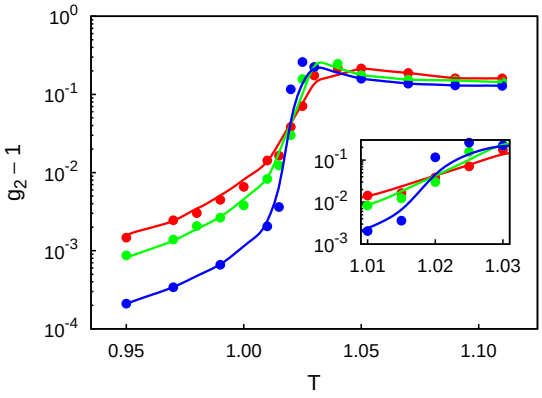

Fig. 2 Plots of second-order cumulants g_2 as functions of temperature T for $N = 500$ (●), $N = 1000$ (●), and $N = 5000$ (●).

To estimate T_{IN} (and therefore S_{IN}) we resort to FSS theory and compute g_2 from eqn. (25) using $\overline{S_b^n} = \langle S_b^n \rangle$ for three system sizes corresponding to $N = 500$, $N = 1000$, and $N = 5000$ mesogens. That data obtained for these system sizes are significant and meaningful is concluded from the much more detailed analysis of the IN phase transition in the present model conducted earlier by Greschek and Schoen.[31]

Results of the present calculations displayed in Figure 2 indicate that above T_{IN} (i.e., in the isotropic phase), g_2 turns out to be independent of system size as one would expect according to the scaling behavior of $\langle S_b \rangle \propto N^{-1/2}$ and that of $\langle S_b^2 \rangle \propto N^{-1}$.[26,31] As one approaches T_{IN} from above, g_2 first passes through a maximum if N is sufficiently large and then declines sharply with decreasing T where in the nematic phase g_2 turns out to be the smaller the larger N is. Most importantly, however, all three curves plotted in Figure 2 pass through a common intersection demarcating $T_{IN} \simeq 1.02$ according to the discussion in Section 3.2.3.

Equipped with this result and with expressions for a, B, and C [see Equations (22a) and (22b)] we are now in a position to estimate T^* where we find $T^*/T_{IN} \simeq 0.746$. For MBBA, Senbetu and Woo's experimental data allow us to estimate $T^*/T_{IN} \simeq 0.904$ which is of about the same order of magnitude.[39] Thus, we conclude that our combined MMF DFT-LdG-FSS approach provides a sufficiently realistic description of the nematic host phase.

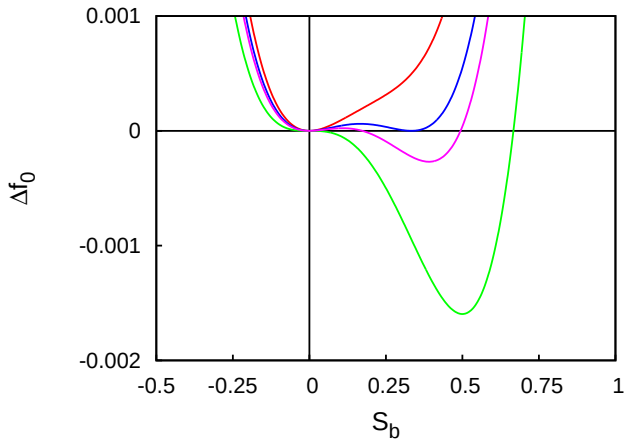

Fig. 3 Plot of the change in LdG free energy density Δf_{LdG} as a function of the nematic order parameter S for $T > T_{IN}$ (——), $T = T_{IN}$ (——), $T < T_{IN}$ (——), and $T = T^*$ (——).

With the parameters T^*, a, B, and C we plot the LdG free energy density Δf_0 from eqn. (13) in Figure 3. As expected, the absolute minimum of Δf_0 corresponds to the isotropic phase ($S_b = 0$) for $T > T_{IN}$. Exactly at $T = T_{IN}$, Δf_{LdG} exhibits a double minimum, one at $S_b = 0$, the other one at $S_b > 0$ in the nematic phase. The depth of both minima is the same, that is isotropic and nematic phases coexist. At T slightly below T_{IN} the depth of the minimum at $S_b > 0$ exceeds that at $S_b = 0$ so that the nematic phase is thermodynamically stable whereas the isotropic phase is only metastable. Finally, at $T = T^*$ the plot of Δf_0 exhibits a saddle point at $S_b = 0$ indicating that the isotropic phase is unstable for all $T \leq T^*$.

4.3 Core region

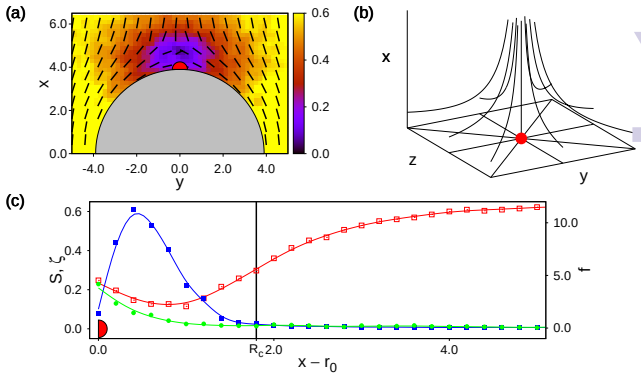

Fig. 4 (a) Director field $\hat{\boldsymbol{n}}(\boldsymbol{r})$ (dashes) and local nematic order parameter $S(\boldsymbol{r})$ (see attached color bar) projected onto the x–y plane. The grey semicircle marks the upper hemisphere of a colloidal particle with part of a Boojum defect topology centered on its north pole. (b) Three-dimensional sketch of the variation of $\hat{\boldsymbol{n}}(\boldsymbol{r})$ for a hyperbolic hedgehog defect topology. (c) Variation of $S(\boldsymbol{r})$ (left ordinate, □), the Frank-Oseen contribution $f_{FO}(\boldsymbol{r})$ [right ordinate, ■, see eqn. (14)], and the biaxial order parameter $\zeta(\boldsymbol{r})$ (left ordinate, see text, ●) as functions of $x - r_0$ and $z = 0$ cutting through the defect core. Notice that the data plotted have been averaged over a strip of width $\delta y = 1.2$ centered on $y = 0$ to get a reasonably smooth variation of all three quantities shown. The vertical solid line marks the radius R_{core} of the circular defect core. Red marks have been added to all three parts of the figure to assist the reader in relating them.

Turning now to our composite system in which colloids are immersed into the nematic host phase, we begin by considering a single colloidal particle first. Plots of the local nematic order parameter $S(\boldsymbol{r})$ and the director field $\hat{\boldsymbol{n}}(\boldsymbol{r})$ in Figure 4(a) reveal the formation of a defect near the colloid's north pole and that this defect is of the Boojum topology as anticipated for a locally planar anchoring of mesogens at the colloid's surface. Upon entering this region, $S(\boldsymbol{r})$ declines sharply so that the defect has a well-defined boundary.

As already mentioned in Section 3.1, special precaution has to be taken to treat the contribution of the defect core to $\Delta f(\boldsymbol{r})$. Within the defect core the variation of $\hat{\boldsymbol{n}}(\boldsymbol{r})$ bears a lot of structural similarity with a hyperbolic hedgehog defect in the bulk [see Figure 4(b)] represented by $\hat{\boldsymbol{n}}(\boldsymbol{r}) = (x, y, -z)^T$ where superscript T denotes the transpose.

Moreover, plots in Figure 4(c) show that outside the defect *core* both $S(\boldsymbol{r})$ and $f_{FO}(\boldsymbol{r})$ vary rather weakly. Hence, the assumption underlying eqn. (14), namely the variation of $\hat{\boldsymbol{n}}(\boldsymbol{r})$ on a length scale exceeding the molecular one, is well justified. Therefore, $f_{el} \approx f_{FO}$ outside the defect core to a good approximation [see eqn. (14)].

Inside the defect core, however, $\hat{\boldsymbol{n}}(\boldsymbol{r})$ varies on a molecular

scale such that $f_{\rm FO}$ passes through a relatively sharp maximum and then declines sharply as one approaches the center of the core region [see Fig 4(c)] so that the assumption underlying $f_{\rm FO}(\boldsymbol{r})$ is no longer justified. To account for the free-energy contribution of the defect core we therefore resort to a procedure suggested earlier by Lubensky *et al.*.[20]

These authors derive an analytic expression for the free energy of defect cores considering analytical director fields (such as the one for the hyperbolic hedgehog defect) [see eqn. (8) of ref.[20]]. Because of the plots in Figure 4(a) and Figure 4(b) we take half of this free energy and assign it to a spherical core volume $\frac{4}{3}\pi R_{\rm core}^3$ to obtain a free-energy density of $f_{\rm core} = K/R_{\rm core}^2$ where $R_{\rm core}$ is the radius of a circular Boojum defect core. We determine the size of the core region by cutting through the center of the defect core of an isolated colloid along the x-axis and take as $R_{\rm core}$ that value of x at which $S(\boldsymbol{r})$ drops below $S_{\rm IN}$ for the first time. Using $R_{\rm core} \simeq 1.80$ [see Figure 4(c)] we obtain $f_{\rm core} \approx 0.50 k_{\rm B}T$ which is not an unrealistic value as we conclude by comparison with the much more sophisticated DFT study of defect-core free-energy densities of de las Heras *et al.*[22]

To approximate the free-energy density of more complex defect topologies to be discussed in Section 4.4 we assume that $f_{\rm core}$ is the same everywhere in the core region irrespective of the defect topology. Hence, the free energy of the defect core is obtained from the expression

$$\mathscr{F}_{\rm core} = f_{\rm core} \int_{V_{\rm core}} {\rm d}\boldsymbol{r} = f_{\rm core} V_{\rm core} \qquad (27)$$

where $V_{\rm core} = \{\boldsymbol{r} | S(\boldsymbol{r}) \leq S_{\rm IN}\}$ is the total volume of the defect core. In practice, we determine $V_{\rm core}$ by partitioning the entire system into small cubes of side length $\delta s = 0.2$ and count the number of cubes in which $S(\boldsymbol{r}) \leq S_{\rm IN}$. The total volume of all these small cubes is then equal to $V_{\rm core}$. In a similar fashion we compute $\Delta f(\boldsymbol{r})$ for small equally sized volume elements and obtain $\Delta\mathscr{F}$ through a three-dimensional integration of $\Delta f(\boldsymbol{r})$ along the x-, y-, and z-axis using a simple trapezoidal rule.

However, it needs to be stressed that this is truly only a rough approximation to the free energy of defect cores even though it is a standard one in the literature.[20,33] Perhaps the most significant assumption behind the expression in eqn. (27) is that of insensitivity of $f_{\rm core}$ to variations in the topology of defects as illustrated by plots in Figure 4. To improve this situation one could *in principle* invoke the approach of Lubensky *et al.*[20] and try to find an analytic expression for $\widehat{\boldsymbol{n}}(\boldsymbol{r})$ inside the defect core such that for each and every topology observed a different $f_{\rm core}$ might obtain analytically. However, if and to what an extent this is possible is currently unknown and would require a study in its own right.

Nevertheless, we feel that the assumption of a assigning the same constant $f_{\rm core}$ regardless of the specific defect topology is not unrealistically crude. This is concluded from the work of Lubensky *et al.*[20] who show that even for rather disparate $\widehat{\boldsymbol{n}}(\boldsymbol{r})$ the free energy of the defect core is more or less the same such that $\mathscr{F}_{\rm core} \propto V_{\rm core}$ to a reasonable degree.

4.4 The effective interaction potential

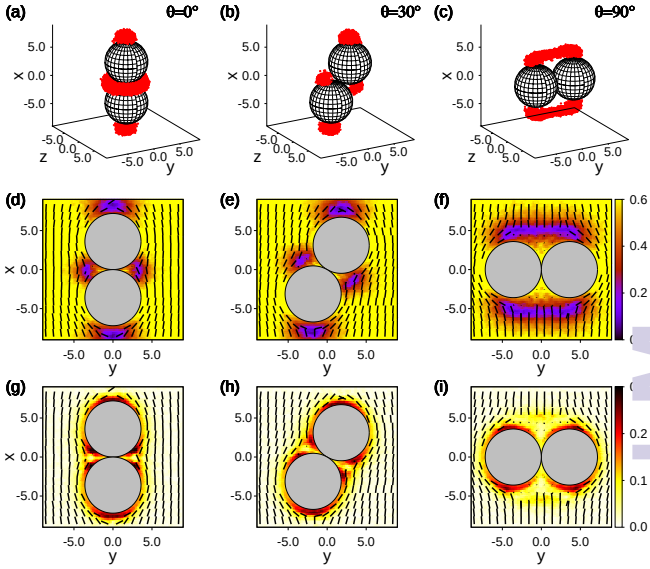

Fig. 5 Upper panel (a)–(c) shows plots of the three-dimensional defect topologies of a pair of colloids (grey spheres) immersed in a nematic host fluid for various angles θ between the center-of-mass distance vector $\boldsymbol{r}_{12}$ and the far-field nematic director $\widehat{\boldsymbol{n}}_0$ given in the plots. Defect regions are colored in red subject to the condition $S(\boldsymbol{r}) \leq \frac{1}{3}$. Plots in the middle panel (d)–(f) show the corresponding local director field (dashes) and the local nematic order parameter (see attached color bar) projected onto the x–y plane where grey circles are similar two-dimensional projections of the colloids. Plots of the biaxiality order parameter are shown in the lower panel (g)–(i). In all cases $\widehat{\boldsymbol{n}}_0 \cdot \widehat{\boldsymbol{e}}_{\rm x} = 1$.

Based upon results presented in Sections 4.2 and 4.3 we now focus on the effective interaction between a pair of colloids immersed in the nematic bulk host phase. We begin in Figure 5 by considering a pair of colloids in contact with each other. Plots (a)–(c) in the upper panel of Figure 5 indicate that part of the Boojum defects at isolated colloids interact at sufficiently close proximity of these colloids. For example, for an angle $\theta = 0°$ between the intercolloidal center of mass distance $\boldsymbol{r}_{12}$ and the far-field nematic director $\widehat{\boldsymbol{n}}_0$ a toroidal defect structure exists surrounding the point of contact between the colloids. As θ increases this torus is first "ripped apart" and eventually a handle-like structure forms at $\theta = 90°$.

Plots (d)–(f) in the middle panel of Figure 5 are projections of $\widehat{\boldsymbol{n}}(\boldsymbol{r})$ onto the x–y plane for the same angles as in parts (a)–

(c) of the same figure. These plots indicate that $\widehat{\boldsymbol{n}}(\boldsymbol{r}) = \widehat{\boldsymbol{n}}_0$ except in the immediate vicinity of the colloidal pair. As one approaches the colloids, $\widehat{\boldsymbol{n}}(\boldsymbol{r})$ is deformed with respect to $\widehat{\boldsymbol{n}}_0$.

Finally, we plot in parts (g)–(i) of Figure 5 the local biaxiality order parameter $\zeta(\boldsymbol{r})$. We compute this quantity from our MC simulations via the smallest and middle eigenvalue of $\mathbf{Q}(\boldsymbol{r})$ in eqn. (17) which can be expressed as $\lambda_- = -[S(\boldsymbol{r}) + \zeta(\boldsymbol{r})]/2$ and $\lambda_0 = -[S(\boldsymbol{r}) - \zeta(\boldsymbol{r})]/2$, respectively, for a system with biaxial symmetry because $\mathrm{Tr}\,\mathbf{Q}(\boldsymbol{r}) = 0$. From Figure 5(g)–5(i) one notices that biaxiality is relatively small and restricted to the immediate vicinity of the colloids' surfaces. We ascribe this to the nanoscopic size of our colloids (i.e., to the large curvature of their surfaces). A comparison with plots in Figure 5(d)–5(g) illustrates the structural similarity between both sets of plots. More specifically, where $S(\boldsymbol{r})$ is lowest, $\zeta(\boldsymbol{r})$ is largest.

This also offers another route to treating $\mathscr{F}_{\mathrm{core}}$ at least *in principle* because the plots in Figure 5 suggest that inside the defect core $\mathbf{Q}(\boldsymbol{r})$ remains non-singular. Instead of invoking the approximations introduced in Section 4.3 one could therefore try to use directly $\mathbf{Q}(\boldsymbol{r})$ from eqn. (17) obtained in the MC simulations and plug it into the right-hand side of the expression on the first line of eqn. (14). The required differentiation of $\mathbf{Q}(\boldsymbol{r})$ has, of course, to be performed numerically but would allow one to compute $f_{\mathrm{el}}(\boldsymbol{r})$ also inside the defect core.

Unfortunately, *in practice* we found that our data are way too noisy to follow this route and obtain reliable values for $f_{\mathrm{el}}(\boldsymbol{r})$ inside the defect core. A reliable numerical differentiation of $\mathbf{Q}(\boldsymbol{r})$ would need a much finer discretization of the grid on which this quantity is stored because of its rather strong spatial variation inside the defect core. Notice, that this does not contradict the smoothness of plots in Figure 4(c) as the data shown there have been averaged over a fairly wide strip inside the defect core.

The magnitude of the spatial variation of $\mathbf{Q}(\boldsymbol{r})$ is reflected in part by the plot of $f_{\mathrm{FO}}(\boldsymbol{r})$ in Figure 4(c) sufficiently deep inside the defect core. In this region, $f_{\mathrm{FO}}(\boldsymbol{r})$ exceeds its typical values in the elastic regime just outside this region by about two to three orders of magnitude. As is clear from eqn. (14) the large value of $f_{\mathrm{FO}}(\boldsymbol{r})$ can immediately be traced back to a very strong spatial variation of $\widehat{\boldsymbol{n}}(\boldsymbol{r})$ inside the defect core which is linked to a similarly strong spatial variation of $\mathbf{Q}(\boldsymbol{r})$ because of eqn. (9).

Consequently, to be able to differentiate this quantity numerically and reliably would require a better resolution of $\mathbf{Q}(\boldsymbol{r})$ on a much finer grid. This obviously would entail much longer MC simulations to obtain reasonably good statistics which, unfortunately, is beyond reach given the number of simulations and the typical system sizes necessary to map out the effective interaction potential between the colloidal pair with sufficient resolution. Because of these constraints and because of the discussion in Section 4.3 we conclude that our present treatment of the free-energy contribution of the defect core offers the best possible approximation.

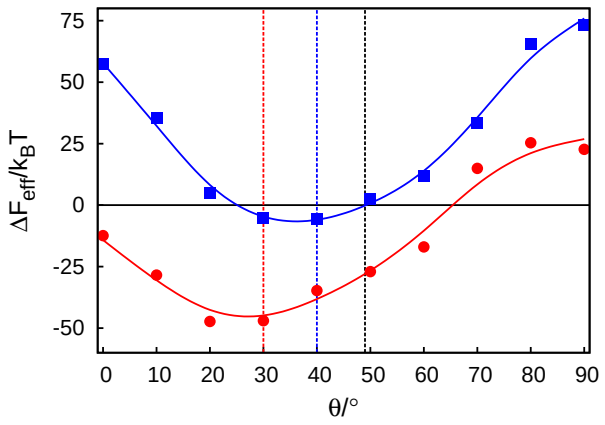

Fig. 6 The effective free energy $\Delta\mathscr{F}_{\mathrm{eff}}$ in units of the change in free energy associated with an isolated Boojum colloid $\Delta\mathscr{F}_{\mathrm{B}}$. Vertical dashed lines demarcate minima in the curves plotted; the limiting value $\theta \approx 49°$ is also indicated (see text); $r_{12} = 7.20$ (●), $r_{12} = 8.00$ (■)

In addition to a distortion of $\widehat{\boldsymbol{n}}(\boldsymbol{r})$ plots in Figures 5(d)–5(f) reveal regions in which $S(\boldsymbol{r}) \ll S_{\mathrm{b}}$. From the parallel three-dimensional plots in Figures 5(a)–5(c) one sees that the volume of these regions changes with θ. Hence, it seems intuitive to introduce an associated change in *effective* free energy

$$\Delta\mathscr{F}_{\mathrm{eff}} = \mathscr{F}_{\mathrm{el}} + \mathscr{F}_{\mathrm{core}} + \Delta\mathscr{F}_{\mathrm{LdG}} - 2\Delta\mathscr{F}_{\mathrm{B}} \qquad (28)$$

where $\Delta\mathscr{F}_{\mathrm{B}}$ is the change in free energy associated with a single Boojum defect. In computing $\Delta\mathscr{F}_{\mathrm{B}}$ we assume that it also consists of an elastic Frank, a defect-core, and a LdG free energy contribution. In practice, it turns out that the contribution of each of the first three terms on the right-hand side of eqn. (28) for the interacting colloidal pair relative to the corresponding contribution to $\Delta\mathscr{F}_{\mathrm{B}}$ is roughly of the same order of magnitude in the range of $k_{\mathrm{B}}T$ in agreement with plots presented in Figure 6 and in Figure 7.

Data for $\Delta\mathscr{F}_{\mathrm{eff}}$ plotted in Figure 6 exhibit a number of interesting features. First, one notices that depending on θ, the sum $\mathscr{F}_{\mathrm{el}} + \mathscr{F}_{\mathrm{core}} + \Delta\mathscr{F}_{\mathrm{LdG}}$ may be larger or smaller than $2\Delta\mathscr{F}_{\mathrm{B}}$ and therefore $\Delta\mathscr{F}_{\mathrm{eff}}$ may be viewed as a repulsive or attractive *effective* interaction potential acting between a colloidal pair and mediated by the nematic host phase. Second, the minimum in the plot of $\Delta\mathscr{F}_{\mathrm{eff}}$ shifts to larger angles θ_{min} as the intercolloidal center-of-mass distance increases. This is fully in line with experimental observations made by Smalyukh *et al.*[11] and theoretical observations made by Tasinkevych *et al.*.[8] Third, these latter authors could also demonstrate that their experimental value of θ_{min} increases monotonically to-

wards a limiting value. This limiting value is found by realizing that for a single Boojum defect (corresponding to a sufficiently separated pair of colloids) the spatial variation of the nematic director field bears close resemblance to the spatial variation of the electrostatic field associated with interacting quadrupoles. For the latter the orientation dependence of the electrostatic energy can be cast as

$$U \propto 9 - 90\cos^2\theta + 105\cos^4\theta \qquad (29)$$

from which $\theta_{\min} \approx 49^\circ$ follows without further ado.

One also notices from the plots in Figure 6 an upward shift of the curves that causes larger spatial regions in which the effective potential $\Delta\mathscr{F}_{\rm eff}$ is repulsive. In particular, such a repulsive region exists for angles $\theta \gtrsim 70^\circ$ and $r_{12} = 8.00$. This is fully in line with trajectories of colloids measured by Smalyukh *et al.*[11] by video microscopy and presented in their Figure 2.

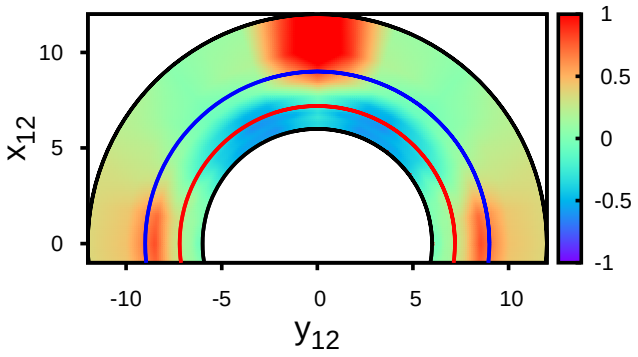

Fig. 7 Contour plot of $\Delta\mathscr{F}_{\rm eff}/\Delta\mathscr{F}_{\rm B}$ (see attached color bar) as a function of $\boldsymbol{r}_{12}^{\rm T} = (x_{12}, y_{12}, 0)^{\rm T}$. Curves plotted in Figure 6 correspond to $r_{12} = 7.20$ (——) and to $r_{12} = 8.00$ (——), respectively.

From curves such as the ones presented in Figure 6 we are now in a position to present in Figure 7 a more refined contour plot of $\Delta\mathscr{F}_{\rm eff}$ illustrating in a broader way the structural complexity of the effective-potential landscape.

Using the data plotted in Figure 7 we can now also investigate structures that several colloids would form in a nematic host phase. For simplicity, and because the experiments used a quasi two-dimensional setup[11] we consider a two-dimensional, coarse-grained system treating the nematic host implicitly via $\Delta\mathscr{F}_{\rm eff}$. To account for the evolution of the colloids in configuration space we employ a conventional canonical-ensemble Metropolis MC scheme.

To that end we store $\Delta\mathscr{F}_{\rm eff}$ on a two-dimensional regular grid with a spacing of 0.2 between neighboring nodes. As a position of a colloid will normally not coincide with a grid point, we interpolate $\Delta\mathscr{F}_{\rm eff}$ between the four nearest-neighbor grid points in a bilinear fashion to get $\Delta\mathscr{F}_{\rm eff}$ at the actual center-of-mass position of a colloidal disk. A displacement of a disk is then accepted with a probability $\min[1, \exp(-\Delta\mathscr{F}_{\rm eff}/\Delta\mathscr{F}_{\rm B})]$.

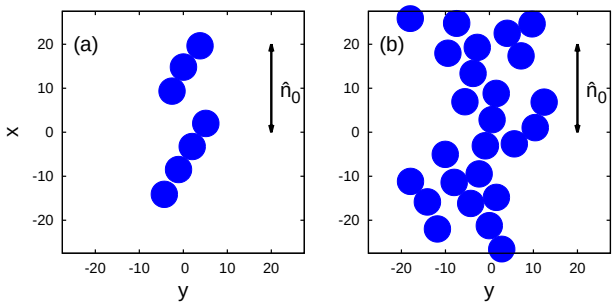

Fig. 8 "Snapshots" from canonical-ensemble MC simulations of colloidal disks immersed in a nematic host phase taken into account implicitly via the effective interaction potential $\Delta\mathscr{F}_{\rm eff}$ shown in Figure 7. (a) $\phi = 0.065$, (b) $\phi = 0.234$ ($s_{\rm x} = s_{\rm y} = 50$ and $\widehat{\boldsymbol{n}}_0 \cdot \widehat{\boldsymbol{e}}_{\rm x} = 1$). The direction of the far-field director $\widehat{\boldsymbol{n}}_0$ is indicated in the figure.

For two packing fractions $\phi = N_{\rm coll}\pi r_0^2/s_{\rm x}s_{\rm y}$ of $N_{\rm coll}$ colloidal disks, characteristic "snapshots" from the simulations at thermodynamic equilibrium are shown in Figure 8. Here $s_{\rm x}$ and $s_{\rm y}$ are linear dimensions of the simulation cell. As one can see colloidal disks tend to form linear chains at the lower packing fraction where the symmetry axis of each chain forms an angle of $\theta \approx 30^\circ$ with $\widehat{\boldsymbol{n}}_0$ [see Figure 8(a)] whereas at higher packing fraction a more extended two-dimensional network of colloidal disks exists at thermodynamic equilibrium [see Figure 8(b)]. Both types of structures bear a remarkable resemblance to those displayed in Figure 1(b) and Figure 1(e) of the work by Smalyukh *et al.*[11]

5 Discussion and conclusions

By means of a novel hybrid approach we investigate the self-assembly of spherical colloidal particles with chemically homogeneous surfaces at a coarse-grained level of description. Our hybrid approach combines molecular-scale methods and theories such as MC computer simulations, classical DFT, and elements of FSS theory with macroscopic theories such as LdG and the Frank-Oseen treatment of the free-energy density associated with elastic deformations of the director field. The goal of this approach is to integrate out less relevant degrees of freedom in a controlled fashion while maintaining the correct physics of a composite system such as the present one. The philosophy of our approach is quite general and may perhaps be applied to other composite systems as well. An example in this respect could be that of Janus colloids immersed into a nematic host phase.

In our case, the colloids are immersed into a nematic liquid-crystal host phase. Self-assembly is driven by effective interactions mediated by the host. The effective iteractions correspond to a change in free energy caused by defects (i.e., regions of lower nematic order) in the host phase. These defects cause a local decline of nematic order and distortion of the director field. Both features arise because of the mismatch between the local alignment of mesogens at the curved surface of the colloids and the nematic far-field director $\widehat{\boldsymbol{n}}_0$. They depend on the arrangement of the colloids in space.

We are treating both the local lowering of nematic order and the distortion of the director field at mean-field level assuming that the former can be adequately accounted for by LdG theory and the latter within the standard expression for the Frank elastic free energy. The mean-field character is reflected by the fact that we compute LdG expansion parameters a, B, and C from mean-field DFT and that the elastic contribution to the change in free energy does not account for fluctuations of $\widehat{\boldsymbol{n}}(\boldsymbol{r})$. However, the Frank free energy is computed only outside the defect core where $\widehat{\boldsymbol{n}}(\boldsymbol{r})$ changes on a length scale large compared to a molecular one.

Applying LdG theory within the framework of molecular simulations poses a fundamental problem because under most conditions statistical accuracy is insufficient to compute the LdG expansion coefficients B and C.[26] However, employing classical DFT allows one to express analytically the LDG coefficients in terms of thermodynamic state parameters such as density and temperature.

A key ingredient in LdG theory is the temperature T^* at which the isotropic phase becomes thermodynamically unstable. It is related to the temperature T_{IN} at which one has IN phase coexistence. To improve our DFT estimate of T^* for the LdG treatment we locate T_{IN} through an analysis of second-order cumulants of the nematic order parameter within the frameowrk of FSS theory.

An alternative route to the LdG coefficients has recently been proposed by Gupta and Ilg.[40] Starting from a state point in the isotropic phase for which they can compute the free energy semi-analytically, Gupta and Ilg apply an external ordering field to drive the system into an ordered nematic phase. In the ordered state the free energy can then be calculated by thermodynamic integration. The intrinsic free-energy contribution can be related to functions that can, on the one hand, be determined *numerically* through reliable fit functions and that one can, on the other hand relate to the LdG expansion coefficients *analytically*.

A crucial ingredient in the approach of Gupta and Ilg is the ordering field which for their Gay-Berne model of a liquid crystal has a magnitude of the order of one. When applying the technique of Gupta and Ilg to our model system we found that the magnitude of the ordering field had to be about five orders of magnitude larger to drive a system from the isotropic to the nematic phase. We believe that this huge difference in the external field is caused by the almost spherical shape of mesogens in our model. Because of the disparate magnitude of the ordering fields it turned out that for the present model the approach of Gupta and Ilg could not be applied reliably.

However, our combined MC-DFT-FSS approach allows us to compute the effective interaction potential reliably. A comparison with experimental data reveals that

1. the effective potential has a minimum at an angle $\theta \approx 30^\circ$ between the intercolloidal distance vector $\boldsymbol{r}_{12}$ and the far-field nematic director $\widehat{\boldsymbol{n}}_0$ if the colloids are sufficiently close to each other.

2. the position of the minimum shifts monotonically to larger θ if r_{12} increases.

3. depending on θ and r_{12} the effective potential may be repulsive or attractive.

These features turn out to be in semi-quantitative agreement with experimental observations.[9,11]

Encouraged by the apparent consistency of these observations with experimental data we perform coarse-grained, canonical-ensemble MC simulations of several colloidal disks immersed in a nematic host phase that is now treated implicitly through the effective interaction potential. In that regard our approach has a multiscale character. The structures observed at different packing fractions agree again qualitatively with experimental data[11] despite the much larger colloids used experimentally.

However, it needs to be stressed that the simulations of several colloids is based upon the assumption of pairwise additivity of the effective interactions. *A priori* there is no guarantee that this assumption is valid. However, the excellent qualitative agreement between structures observed within our approach with those seen experimentalls seems to justfy the assumption of pairwise additive effective interactions *a posteriori*.

In summary, we have shown that the self-assembly of colloidal particles in a nematic liquid crystal is driven by the occurrence of colloid-induced defects associated with a local elastic distortion of the director field. This also implies that in an isotropic phase no such self-assembly would occur as the effective interaction potential would vanish identically.

We are grateful for financial support from the Deutsche Forschungsgemeinschaft via the International Graduate Research Training Group 1524.

References

1 P. G. de Gennes and J. Prost, *The physics of liquid crystals*, Clarendon, Oxford, 2nd edn., 1995.

2 V. S. R. Jampani, M. Škarabot, M. Ravnik, S. Čopar, S. Žumer and I. Muševič, *Phys. Rev. E*, 2011, **84**, 031703.

3 K. Izaki and Y. Kimura, *Phys. Rev. E*, 2013, **87**, 062507.
4 U. Ognysta, A. Nych, V. Nazarenko, M. Škarabot and I. Muševič, *Langmuir*, 2009, **25**, 12092–12100.
5 H. Qi and T. Hegmann, *J. Mater. Chem.*, 2006, **16**, 4197–4205.
6 M. Humar, M. Ravnik, S. Pajk and I. Muševič, *Nat. Photonics*, 2009, **3**, 595–600.
7 I. Muševič, M. Škarabot and M. Humar, *J. Phys.: Condens. Matter*, 2011, **23**, 284112.
8 M. Tasinkevych, N. M. Silvestre and M. M. Telo da Gama, *New J. Phys.*, 2012, **14**, 073030.
9 P. Poulin and D. Weitz, *Phys. Rev. E*, 1998, **57**, 626–637.
10 P. Poulin, H. Stark, T. C. Lubensky and D. A. Weitz, *Science*, 1997, **275**, 1770–1773.
11 I. I. Smalyukh, O. D. Lavrentovich, A. N. Kuzmin, A. V. Kachynski and P. N. Prasad, *Phys. Rev. Lett.*, 2005, **95**, 157801.
12 S. Giura and M. Schoen, *Phys. Rev. E*, 2014, **90**, 022507.
13 W. Maier and A. Saupe, *Z. Naturforsch., A: Phys. Sci.*, 1958, **13**, 564–566.
14 W. Maier and A. Saupe, *Z. Naturforsch., A: Phys. Sci.*, 1959, **14**, 882–889.
15 B. Jérôme, *Rep. Prog. Phys.*, 1991, **54**, 391–451.
16 M. Škarabot, M. Ravnik, S. Žumer, U. Tkalec, I. Poberaj, D. Babič, N. Osterman and I. Muševič, *Phys. Rev. E*, 2008, **77**, 031705.
17 A. A. Sonin, *The Surface Physics of Liquid Crystals*, Gordon and Breach, Amsterdam, 1995.
18 M. Melle, S. Schlotthauer, M. G. Mazza, S. H. L. Klapp and M. Schoen, *J. Chem. Phys.*, 2012, **136**, 194703.
19 R. W. Ruhwandl and E. M. Terentjev, *Phys. Rev. E*, 1997, **56**, 5561–5566.
20 T. C. Lubensky, D. Pettey, N. Currier and H. Stark, *Phys. Rev. E*, 1998, **57**, 610–625.
21 S. Grollau, N. L. Abbott and J. J. de Pablo, *Phys. Rev. E*, 2003, **67**, 011702.
22 D. de las Heras, L. Mederos and E. Velasco, *Liq. Cryst.*, 2010, **37**, 45–56.
23 I. Bajc, F. Hecht and S. Žumer, arXiv:1505.07046v1.
24 J. Dontabhaktuni, M. Ravnik and S. Žumer, *Soft Matter*, 2012, **8**, 1657–1663.
25 I. Muševič, U. Škarabot, U. Tkalec, M. Ravnik and S. Žumer, *Science*, 2006, **313**, 954–958.
26 R. Eppenga and D. Frenkel, *Mol. Phys.*, 1984, **52**, 1303–1334.
27 W. H. Press, S. A. Teukolsky, W. T. Vetterling and B. P. Flannery, *Numerical recipes*, Cambridge University Press, Cambridge, 3rd edn., 2007.
28 M. P. Allen and D. Frenkel, *Phys. Rev. A*, 1988, **37**, 1813R–1816R.
29 M. P. Allen and D. Frenkel, *Phys. Rev. A*, 1990, **42**, 3641.
30 T. Stieger, M. Schoen and M. G. Mazza, *J. Chem. Phys.*, 2014, **140**, 054905.
31 M. Greschek and M. Schoen, *Phys. Rev. E*, 2011, **83**, 011704.
32 S. Giura, B. G. Márkus, S. H. L. Klapp and M. Schoen, *Phys. Rev. E*, 2013, **87**, 012313.
33 M. Kleman and O. D. Lavrentovich, *Soft Matter Physics: An introduction*, Springer-Verlag, New York, 2003.
34 H. Weber, W. Paul and K. Binder, *Phys. Rev. E*, 1999, **59**, 2168–2174.
35 K. Vollmayer, J. D. Reger, M. Scheucher and K. Binder, *Z. Phys. B: Condens. Matter*, 1993, **91**, 113–125.
36 D. Frenkel and B. Smit, *Understanding molecular simulation: From algorithms to applications*, Academic Press, San Diego, 2nd edn., 2002.
37 M. P. Allen and D. J. Tildesley, *Computer simulation of liquids*, Oxford University Press, Oxford, 2002.
38 W. Maier and A. Saupe, *Z. Naturforsch., A: Phys. Sci.*, 1960, **15**, 287–292.
39 L. Senbetu and C.-W. Woo, *Mol. Cryst. Liq. Cryst.*, 1982, **84**, 101–124.
40 B. Gupta and P. Ilg, *Polymers*, 2013, **5**, 328–343.